Renewable Energy 164 (2021) 1108–1120

Contents lists available at ScienceDirect

Renewable Energy

journal homepage: www.elsevier.com/locate/renene

On the design of potential turbine positions for physics-informed optimization of wind farm layout

Chutian Wu [a, b], Xiaolei Yang [a, c, *], Yaxin Zhu [b]

[a] State Key Laboratory of Nonlinear Mechanics, Institute of Mechanics, Chinese Academy of Sciences, Beijing, 100190, China
[b] Department of Mechanics, Huazhong University of Science and Technology, Wuhan, 430074, China
[c] School of Engineering Sciences, University of Chinese Academy of Sciences, Beijing, 100049, China

ARTICLE INFO

Article history:
Received 16 July 2020
Received in revised form
7 October 2020
Accepted 14 October 2020
Available online 21 October 2020

Keywords:
Wind farm layout optimization
Physics-informed
Potential turbine positions
Jensen wake model
Genetic algorithm

ABSTRACT

Wind farm layout optimization is a critical step in the design of a wind energy project. In the literature, the potential turbine positions employed in the layout optimization are often obtained by discretizing the field using a Cartesian mesh. In this work, physical understanding is proposed to incorporate in the design of potential turbine positions. Specifically, the known knowledge, that a staggered arrangement is more efficient for extracting energy from wind than an aligned arrangement, is employed and implemented using the staggered mesh approach, the unstructured mesh approach and the sunflower mesh approach. Different mesh approaches are tested using two cases, i.e. case I, unidirectional uniform wind, and case II, uniform wind with variable wind direction. The optimal layout obtained from the staggered mesh approach performs the best for case I. For case II, the farm performance from different layouts is similar. The performance of the layouts under off-design conditions is also tested for case I. For all considered cases, the optimal layout obtained from the sunflower approach shows an overall good performance.

1. Introduction

Growing as a key player in the world's energy supply, the cost of wind energy has to be further reduced to keep economically competitive [1]. Wind farm layout optimization (WFLO), which can significantly influence the performance of a wind farm, is one critical step in developing a wind energy project. A wind layout optimization approach is often composed of an optimization algorithm, a turbine wake model and objective functions. Optimization algorithms based on discrete variables are often employed in the literature because of the nature of WFLO problems [2–4]. In these approaches, the potential turbine locations are often defined by a Cartesian mesh. Based on the pioneering work by Mosetti et al. [5], in this work physical understanding is proposed to incorporate in the design of potential turbine locations as a first step towards the development of a physics-informed approach for WFLO problems.

The wind turbine positions can be represented using continuous variables or discrete variables. The continuous variable approach allows a turbine to be installed anywhere satisfying certain constraints, while the discrete variable approach only offers a limited number of potential positions. Only a few approaches are based on continuous variables. For instance, Yunus et al. [6] employed an ant colony algorithm based on continuous variables to optimize a wind farm layout with specified number of turbines. The discrete approach has been utilized by many researchers [3–5,7,8] since Mosetti et al. [5], who first introduced the genetic algorithm to WFLO problems. Other optimization algorithms have also been employed in the literature, such as the binary particle swarm optimization by Sittichoke et al. [9], a quadratic integer program and a mixed integer linear program employed by Turner et al. [10]. Compared with gradient-based algorithms often ending at local optimum, genetic algorithm performs better at finding global optimal solutions. However, it also has some drawbacks, such as slow convergence, loss of the best solution, and no assurance that a global optimum will be found [11].

The turbine wake is featured by low wind speed and high velocity fluctuations, which decreases the downwind turbine's power output and increases its fatigue loads. One key objective in WFLO is to minimize the adverse impacts of turbine wakes on wind farm

* Corresponding author. State Key Laboratory of Nonlinear Mechanics, Institute of Mechanics, Chinese Academy of Sciences, Beijing, 100190, China.
E-mail address: xyang@imech.ac.cn (X. Yang).

https://doi.org/10.1016/j.renene.2020.10.060
0960-1481/

performance. The turbine wake can be modeled using computational models of different fidelities ranging from analytical engineering models [12–17], models based on simplified Navier-Stokes equations [18–20], Reynolds-Averaged Navier-Stokes (RANS) models [21–24] to large-eddy simulation (LES) [25–29]. Jensen wake model [12,30] is the one widely used in WFLO problems, which will also be employed in this work. Analytical models have the advantage in terms of computing efficiency, but cannot accurately predict the turbulence statistics in wind farms. High-fidelity models like LES can accurately predict key dynamics of turbulent flows in wind farms, e.g. wake meandering [31], but it is computational prohibitive for WFLO problems. To take into account more physics of turbine wakes, a feasible approach is to incorporate our physical understanding in WFLO instead of directly simulate wake dynamics using high-fidelity models.

It has been shown in the literature numerically [32,33] and experimentally [34,35] that a staggered turbine array can produce more power than an aligned turbine array with the same turbine density, because of larger turbine spacing in the downwind direction as turbines in every other row are offset in the lateral direction. In this work, the knowledge, that a staggered turbine arrangement is more efficient for energy extraction, for designing potential turbine positions. The WFLO method is based on the classic work by Mosetti et al. [5]. The optimization results are compared with those from Grady et al. [7]. It is noted that this work only focuses on the optimization of power extraction. Other costs, such as the installation and transportation cost and the operation & maintenance cost, and restrictions related with technical feasibility especially for offshore wind [36], are not considered.

The rest of the paper is organized as follows. The approach employed for WFLO is described in section 2. Then, the optimization results are presented in section 3. At last, conclusions from this work are drawn in section 4.

2. Staggered mesh approach for physics-informed optimization

The key idea of this work is to take into account the physics for optimizing the wind farm layout in order to obtain wind farm layout solutions closer to the global optimal solution. Specifically, the staggered arrangement for discretizing the wind farm site, which has been shown having better performance than the aligned arrangement, is considered. In this section, the employed staggered arrangement is first described in section 2.1, Jensen wake model and the genetic algorithm are then presented in sections 2.2 and 2.3, respectively.

2.1. Staggered arrangement for discretizing the site

Two ideal scenarios, i.e. 1) uniform wind blowing only in one direction, 2) uniform wind blowing evenly from all directions, are considered. For the first scenario, the staggered arrangement can be easily realized using a simple staggered mesh as shown in Fig. 1(a). As seen, in the staggered mesh approach, the potential turbine positions are defined by shifting every other row right by half grid width. For the second scenario, a grid staggered for all wind direction cannot be easily obtained. Two options, i.e. the unstructured mesh approach and the sunflower mesh approach, are explored. In the unstructured mesh approach, the site is discretized by unstructured triangular cells with potential turbine locations defined at cell centers. In the sunflower approach the potential turbine positions are specified in a way the same as the pattern of seeds in a sunflower, which is given in polar coordinates r, ϕ, for the k^{th} position as follows [37]:

$$\phi_k = k137.5^\circ, r_k = a\sqrt{\phi_k}, \tag{1}$$

where angle 137.5° is often observed in the pattern of sunflower seeds as well as in the arrangement of leaves, the lateral growth program $r_k = a\sqrt{\phi_k}$ ensures an equal area for each seed, and a is the parameter for controlling the size of the area. In the staggered mesh approach, the potential turbine locations are perfectly staggered for wind in the north-south directions. The unstructured mesh approach and the sunflower mesh approach are intended to provide staggered arrangement for wind blowing from different directions.

Considering only the above two ideal scenarios is because of the lack of an approach for generating optimal potential turbine positions for complex wind conditions with non-uniform distributions of wind speed and wind roses. The employed staggered mesh is staggered in one direction. The other three meshes, on the other hand, are approximately isotropic and homogeneous, which are expected being ideal for uniformly distributed wind directions (this needs to be examined further). The basic idea of the proposed approach is to introduce staggered arrangement in the design of potential turbine positions. It is straightforward for the first scenario. For the second scenario, the unstructured mesh and the sunflower mesh are just two attempts to introduce some degree of staggering. For realistic wind conditions with varying wind speed and complex wind roses, simply employing non Cartesian meshes is not enough for the design of optimal potential turbine positions. To develop a general approach for the design of potential turbine, a measure for the degree of staggering (or other physics) has to be developed first. With this measure, the optimal potential turbine positions can then be designed for the optimization of wind farm layouts.

2.2. Jensen wake model

One of the widely used wake models is Jensen wake model [12,30]. With the momentum conservation and the assumption of linear wake expansion, Jensen wake model gives the velocity u in the wake as follows:

$$\frac{u}{u_0} = 1 - \frac{2a}{(1 + \alpha x/r_1)^2}, \tag{2}$$

where u_0 is the undisturbed incoming wind velocity, x is the downstream distance from the turbine, a is the axial induction factor, α is the entertainment constant, and r_1 is the initial radius of the wake. The entertainment constant α, which describes the growth rate of the wake width, is given by the following empirical relation:

$$\alpha = \frac{0.5}{\ln(z_h/z_0)}, \tag{3}$$

where z_h is the hub height and z_0 is the surface roughness length. The initial wake radius r_1, which is derived based on the one-dimensional momentum theory, is computed as follows:

$$r_1 = r\sqrt{\frac{1-a}{1-2a}}, \tag{4}$$

where r the radius of the rotor. The employed Jensen model is the same as the one employed by Frandsen [30], which is different from the model presented in Jensen's paper [12] in the way how to calculate the entrainment constant α and initial radius of the wake r_1. A typical wind speed distribution in turbine wake predicted by

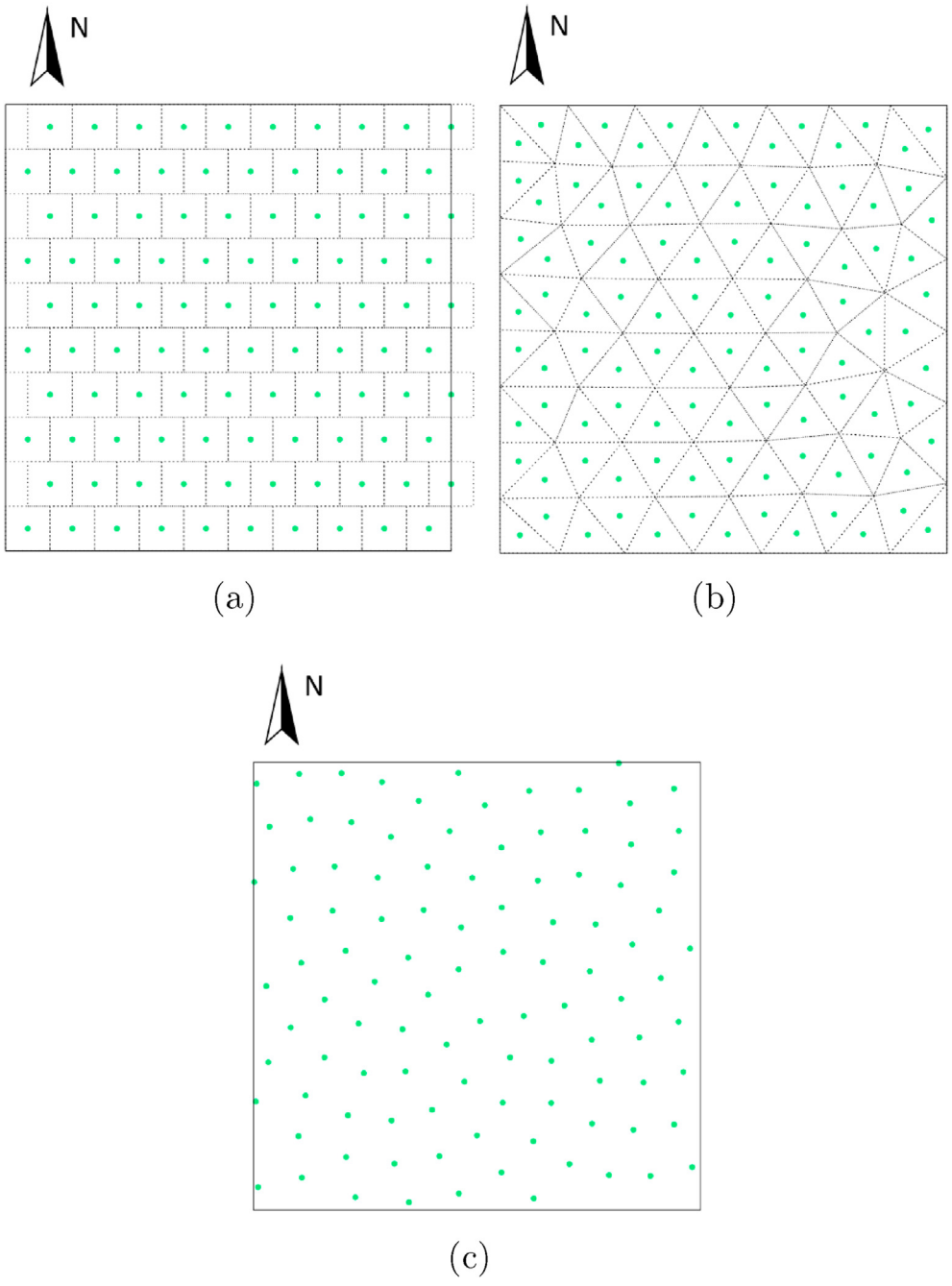

Fig. 1. Potential turbine positions (green points) defined using different approaches for (**a**) the staggered mesh approach, (**b**) the unstructured mesh approach, and (**c**) the sunflower mesh approach, respectively. (For interpretation of the references to colour in this figure legend, the reader is referred to the Web version of this article.)

Jensen wake model is shown in Fig. 2.

In order to account for the effects of wakes from upwind turbines on velocity deficit, the quadratic sum method [38] is used, in which the wind speed u_i at turbine i is calculated as:

$$\left(1-\frac{u_i}{u_0}\right)^2=\sum_j^n\left(1-\frac{u_{ij}}{u_0}\right)^2, \tag{5}$$

where u_{ij} is the wind speed at turbine i due to wake of turbine j, and the summation is taken over the n turbines upwind of turbine i. Different wake models can also be employed. Reviews on different types of modeling methods can be found in Ref. [39–42].

In this work, the same turbine as that in Ref. [5,7] is employed, which has a hub height of 60 m and a rotor diameter of 40 m. The surface roughness length z_0 is 0.3 m. The turbine operational condition is also the same as that in Ref. [5,7], that the thrust coefficient is $C_T = 0.88$ and the power curve is given as follows:

$$P = 0.3u^3 \text{ kW}, \tag{6}$$

thus the total power extracted by the wind farm is calculated as

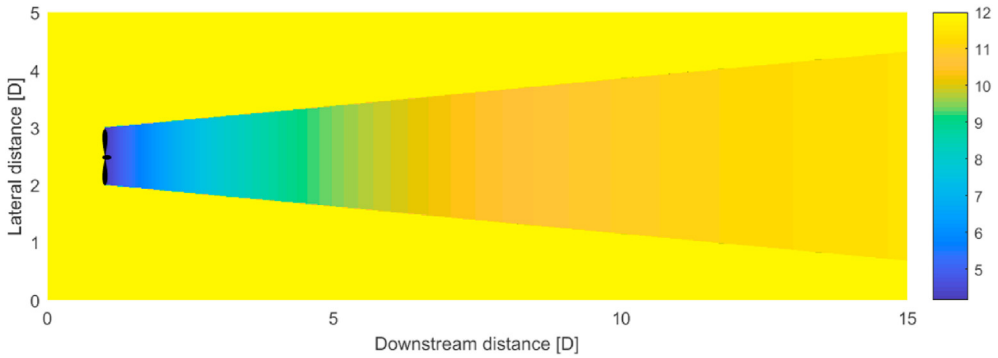

Fig. 2. Contour of axial wind speed in turbine wake predicted by Jensen wake model, in which $u_0 = 12$ m/s, $a = 0.33$, and $\alpha = 0.0944$.

follows:

$$P_{\text{total}} = \sum_{i}^{N} 0.3u_i^3 \text{ kW}, \tag{7}$$

where N is the total number of turbines. With C_T, the axial induction factor $a = 0.33$ is obtained using the relation $C_T = 4a(1-a)$ for the wake deficit calculation using Eq. (2)

2.3. Optimization method

Genetic algorithm for wind farm optimization as in Ref. [5,7], which searches for the optimal solution by simulating Darwinian natural evolution and genetic process. In genetic algorithm, the individuals in a population which have the best fitness are more likely to reproduce and impart their genetic information to the next generation. As the process goes on, the genes which controls better traits are inherited and the mean fitness of a population increases. The elemental steps of genetic are Selection, Crossover, Mutation, and Reinsertion, which are described in detail in Ref. [11].

As shown in Fig. 3, in WFLO problems, given the characteristics of a potential wind farm site including the location, area, terrain, wind and other constraints, potential turbine positions using a physics-informed approach, e.g. the one described in section 2.1, are first designed. Having these potential turbine positions, a population of many different turbine layouts are generated, which are binary arrays of 0s (no turbine) and 1s (turbine). The power outputs of different layouts are calculated based on Jensen wake model as described in section 2.2. The fitness of different layout is evaluated based on the objective function, which will be described later. According to fitness, parents are then selected to create new generation of turbine positions using the genetic manipulation. If the optimization criteria is not met, the above iteration will be repeated. In the end of this procedure the optimal turbine positions giving the best fitness will be obtained. The total number of turbines, which is not specified in the optimization process, is also an output from this procedure. To design a wind farm, people often have little or no information on the best number of turbines to be installed. Fixing the number of turbines to be installed based on the rated power capacity of a wind farm may overestimate or underestimate the full potential of wind energy that can be tapped [43]. On the other hand, having the number of turbines as a variable to optimize in WFLO problems enable the possibility for an optimal layout, which fully utilizes the energy potential of the site and minimizes the negative effects of turbine wakes at the same time.

Different objective functions have been used the literature [11]. In this work, the objective function as in Ref. [5,7] is employed, which is chosen as the cost per unit power produced shown as follows:

$$Obj = \frac{\text{cost}}{P_{\text{total}}}, \tag{8}$$

where the total cost per year is given by Ref. [5].

$$\text{cost} = N\left(\frac{2}{3} + \frac{1}{3}\exp\left(-0.00174N^2\right)\right), \tag{9}$$

which is non-dimensionalized using the annual cost of a single turbine, and assumes a maximum cost reduction of 1/3 for each turbine [5].

3. Results and discussions

Two cases the same as those reported by Grady et al. [7], i.e. case

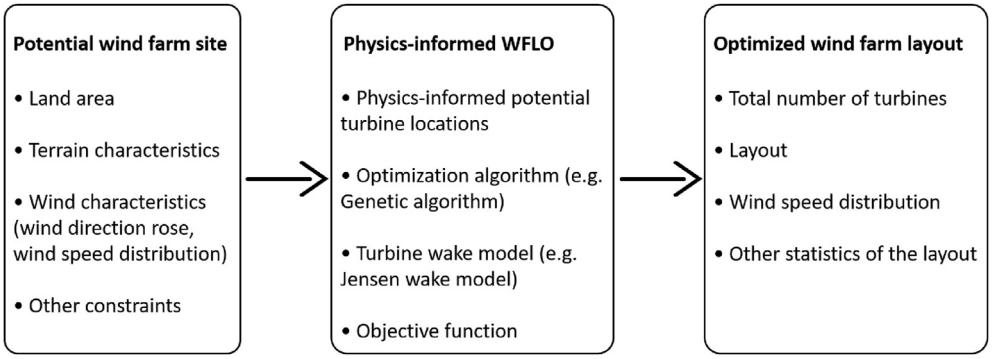

Fig. 3. A flowchart of the present wind farm layout optimization approach.

I, unidirectional wind comes with a constant speed of $u_0 = 12$ m/s, and case II, uniform wind comes from various direction with the same probability, are considered. In case II the wind direction is discretized into 36 segments when optimizing the wind farm layout. The size of the wind farm is $50D \times 50D$. For the aligned and staggered configurations, there are 100 potential turbine positions. The unstructured and sunflower configurations are designed in a way that the total numbers of potential turbine positions, which are 102 and 103 potential turbine positions, respectively, are approximately the same as that of the aligned and staggered configurations.

3.1. Case I: unidirectional uniform wind

To validate the implementation of the present WFLO code, the results of the aligned case computed in this work are compared with those from Grady et al. [7]. As seen in Fig. 4(a), the turbine positions computed from the present work are identical with those from Grady et al.'s work [7]. When potential positions are aligned, a clear left-right symmetry of the obtained turbine layout is observed with the 1^{st} row of turbines located in the first row of the grid nodes to extract maximal power from the free wind, and the 2^{nd} and the 3^{rd} rows of the turbines located in the 6^{th} and the last rows of the grid nodes, respectively, to minimize the overall impacts of the 1^{st} row turbine wakes on the second row turbines, and the 2^{nd} two turbine wakes on the last row turbines, and achieve an optimal balance between wake interaction and power production. The turbine layout from the staggered case as shown in Fig. 4(b), on the other hand, is significantly different, with 20 turbines located in the very front of the domain and 20 turbines located in the end of the domain, respectively. With such staggered arrangement, turbines in the first two rows can extract the most power from free incoming wind and reduce the impacts of their wakes on downwind turbines. The turbine layout obtained from the unstructured mesh is shown

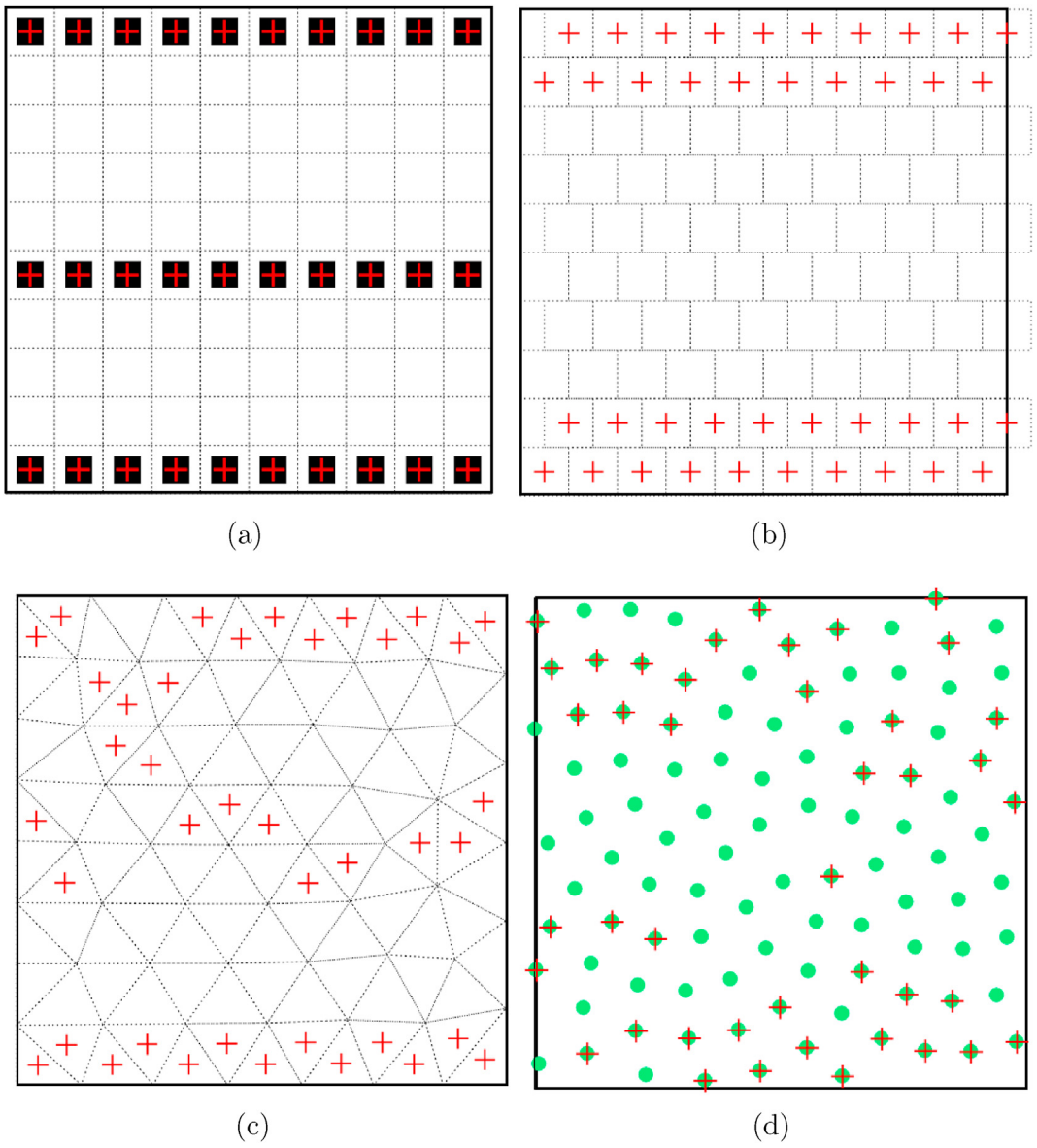

Fig. 4. Optimal layouts obtained from different potential turbine positions for (a) aligned mesh, (b) staggered mesh, (c) unstructured mesh and (d) sunflower mesh, respectively for case I. Filled squares: Grady et al. [7]; Red crosses: present results; Green dots: potential positions for the sunflower mesh approach. (For interpretation of the references to colour in this figure legend, the reader is referred to the Web version of this article.)

in Fig. 4(c). As seen, the turbine positions are not as organized as those from the aligned and staggered cases. But if one examines more carefully, it can be observed that the layout from the unstructured case has some common features with the aligned and staggered cases, that the turbines in the front and the rear of the domain are placed in a staggered way as those obtained from the staggered case, and some turbines are located in the middle of the domain similar to that observed in the layout from the aligned case. The layout obtained from the sunflower case is shown in Fig. 4(d). It is seen that the obtained layout, which has a dumbbell shape with most turbines located in the front and rear of wind farm, is significantly different from those from the other three cases.

The characteristics of the optimal layouts obtained from different cases are compared in Table 1. As seen, the efficiency of the optimal layout (which is defined as $\eta = \frac{P_{\text{total}}}{N0.3u_0^3}$) from the unstructured mesh case is similar with that from the aligned mesh case. The efficiencies of the optimal layouts from the staggered and sunflower cases, on the other hand, are about 5% and 2% higher than those from the aligned and unstructured case, respectively, with the staggered mesh configuration having the highest efficiency. Furthermore, it is observed that the optimal total numbers of turbines from the staggered, unstructured and sunflower cases are about 30% larger than that from the aligned mesh case without impairing the layout efficiency. An ideal value of the objective function, i.e. $Obj_{\text{ideal}} = 1.2860 \times 10^{-3}$ kW^{-1}, can be obtained by assuming all turbines facing free wind and finding the limit of the following objective function

$$Obj = \frac{N\left(\frac{2}{3} + \frac{1}{3}\exp\left(-0.00174N^2\right)\right)}{0.3u_0^3 N} = \frac{1}{0.3u_0^3}\left(\frac{2}{3} + \frac{1}{3}\exp\left(-0.00174N^2\right)\right) \quad (10)$$

for $N \to \infty$, where $u_0 = 12$ m/s for the present cases As seen, compared with the optimal solution of Grady et al. [7], the optimal layout from the staggered case is closer to the ideal optimal solution. It should be noted that the performance improvement of 2%–5% is significant for the revenue of a utility-scale wind farm as estimated by Pao and Johnson [44] for turbine control algorithms. The *Obj* value obtained in this work is lower than that obtained by Marmidis et al. [45] for the same case, in which $Obj = 1.4107 \times 10^{-3}$ for $N = 32$, and that in Ref. [46], where $Obj = 1.5414 \times 10^{-3}$ for $N = 31$. The efficiency of the present optimal layout is better than or similar with that in the literature. For instance, an increase of 3.2% in the produced power is observed in the paper by González et al. [47] as compared with Grady et al.'s results [7]. In the work by Pookpunt and Ongsakul [48], the obtained efficiency is 92.01%, which is lower than that obtained from the staggered mesh and the sunflower mesh.

Table 1
Characteristics of the optimal layouts obtained from different configurations of potential turbine positions for case I. It is noticed that the unit of *Obj* is 1/kW because that the cost computed using Eq. (9) is non-dimensionalized using cost/year of a single turbine.

	Aligned [7]	Staggered	Unstructured	Sunflower
Obj (1/kW, $\times 10^{-3}$)	1.5436	1.3816	1.4470	1.3941
P_{total}(kW)	14310	19898	18605	20551
η (%)	92.02	96.96	92.03	94.39
N	30	40	39	42

The wind fields from different optimal layouts are examined in Fig. 5. As seen in Fig. 5(a) for the aligned case, all turbines in the second and third rows are positioned in wakes from upwind turbines. For the layout from the staggered case, on the other hand, the wake effects are significantly less because of the larger turbine spacings in the downwind direction. For the unstructured and sunflower approach, the wind distributions are more complicated than the other two with the possibility that the rotor of one turbine might be partially located in the near wake of its upwind turbines as the incoming velocity at the center of the rotor is employed without taking into account the distribution of the incoming velocity on the rotor disk.

3.2. Case II: uniform wind with variable wind direction

In this section, the four different configurations for potential turbine locations are applied to the case with uniform wind evenly blowing from different wind directions. The same has been carried out by Grady et al. [7] using an aligned mesh. As shown in Fig. 6(a), differences between the present result and that from Ref. [7] are observed. In the present results, more turbines are located around the boundary, while in Grady et al.'s results [7], the turbines are distributed in a way close to uniform. The optimal layouts obtained from the other three meshes for potential turbine positions are shown in Fig. 6(b), (c), and 6(d). The turbine positions from the three meshes are completely different but with one common feature that about 65% of the turbines are located along the boundary.

In Table 2, the performance of the optimal layouts obtained from different configurations of turbine potential positions is compared. It is seen that the efficiencies of the optimal layouts obtained in the present work are approximately 2% more than that from Grady et al. work [7]. It is also observed the optimal layouts from the aligned, unstructured and sunflower meshes have 2 more turbines than the unstructured mesh and those from Grady et al. [7] and others [49,50]. As the *Obj* values are very similar for different meshes and smaller than that from Grady et al. [7], this increase of 2 more turbines is justified for the simple cost model employed in this work. For complex cost models considering other aspects such as the fatigue loads and the foundation cost for offshore wind, the present optimal layouts need to be further examined and the corresponding optimal layouts can be significantly different from those designed using the simple cost model.

Fig. 7 shows the wind field for different optimal layouts. It is seen that the contours of the downwind velocity for the optimal layouts from the staggered mesh, the unstructured mesh and the sunflower mesh are more complicated than that from the aligned mesh, in which less turbines are located in the middle of the domain.

3.3. Performance for off-design conditions for case I

The real wind environment is very complicated. For a wind farm site with a prevailing wind direction, it is still possible that the wind blows from different wind directions. Thus, it is important to further examine the performance of the optimal layout, which only considers the prevailing wind direction. In this section, the performance of the optimal layouts obtained from case I under an off-design condition is examined. The turbine layouts examined are shown in Fig. 4, which are optimized for wind from the north direction using the four different meshes. In the considered off-design condition, the wind blows from the east direction with the same wind speed of 12 m/s as in case I. The turbine also operates

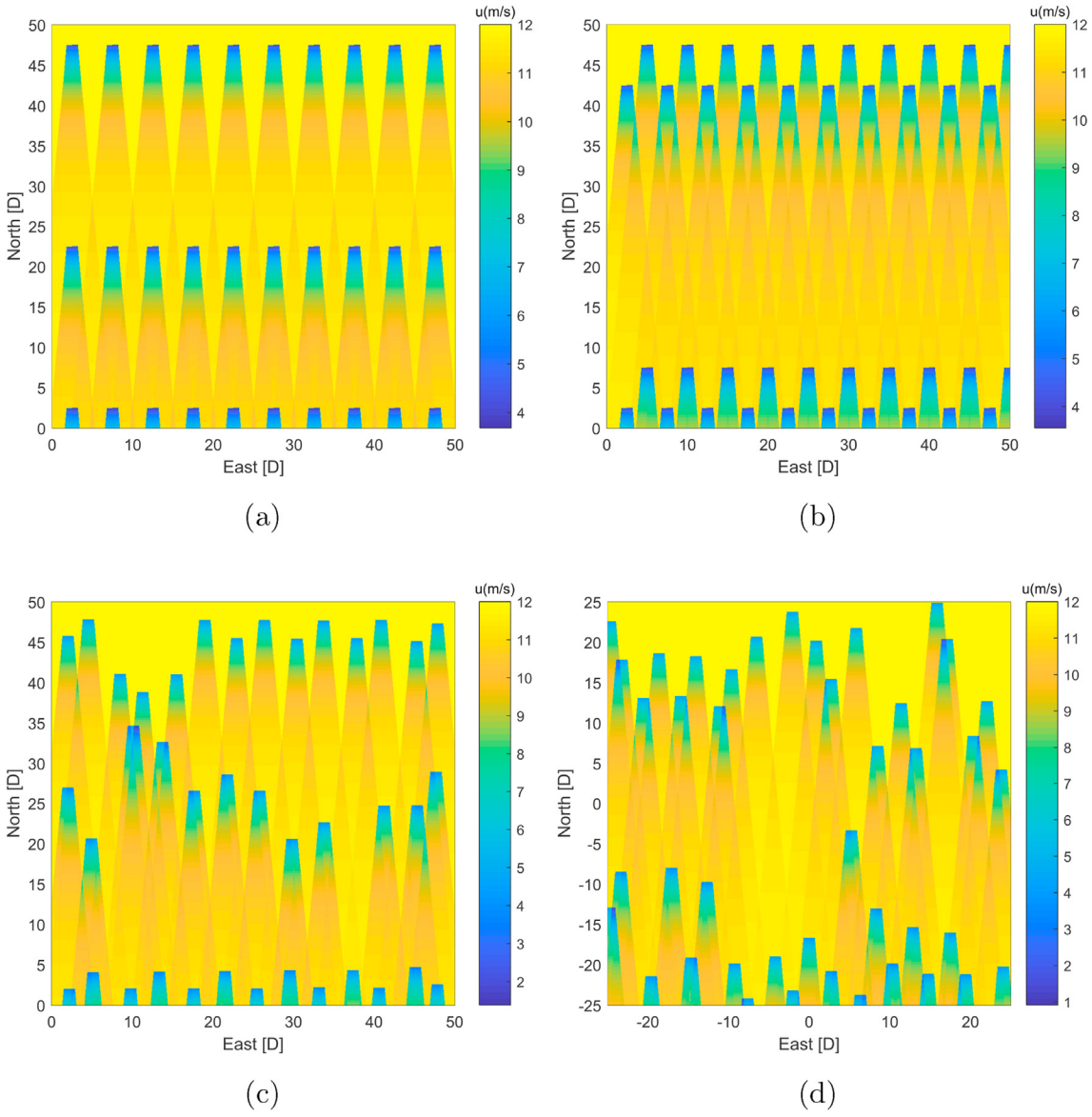

Fig. 5. Contours of downwind velocity for different optimal layouts for (a) optimal layout from the aligned mesh, (b) optimal layout from the staggered mesh, (c) optimal layout from the unstructured mesh, and (d) sunflower, respectively for case I.

under the same condition as in case I with its power computed using Eq. (6).

The off-design performance of the four optimal layouts obtained for case I is presented in Table 3. As seen, the efficiencies are reduced by half for the optimal layouts from the aligned and staggered meshes. The efficiencies of the optimal layouts from the unstructured and sunflower meshes, on the other hand, are still more than 75% of the efficiency for the design condition. The corresponding wind fields from different layouts are shown in Fig. 8. It is obvious that significant reductions on the efficiency for the optimal layouts from aligned and staggered meshes are caused by large velocity deficits because of small turbine spacings along the east-west direction. It is noticed that this is an extreme off-design condition that the wind blows in a direction perpendicular with the prevailing wind direction. For other off-design wind directions, the performance of optimal layouts obtained from the aligned and staggered meshes may not be reduced that much. Since the wind comes parallel to the staggered displacement in the staggered configuration, it turns to be same configuration as the aligned, that the same efficiency is shared. Turbines are arranged right in wakes on the aligned and staggered configuration, which makes a significant power loss. Due to the configuration that positions are staggered in every direction, the sunflower has the best performance under this off-design condition.

For off-design conditions, turbine wakes play a more important role on the power production and dynamic loads on downwind turbines. For the layouts from the aligned and staggered meshes, except for the very upwind turbines, all other turbines are fully immersed in wakes of their upwind turbines. For the layouts from other two meshes especially for that from the sunflower mesh, only several turbines are fully immersed in wakes of their upwind turbines. Velocity deficits in turbine wakes reduce energy available for downwind turbines and thus

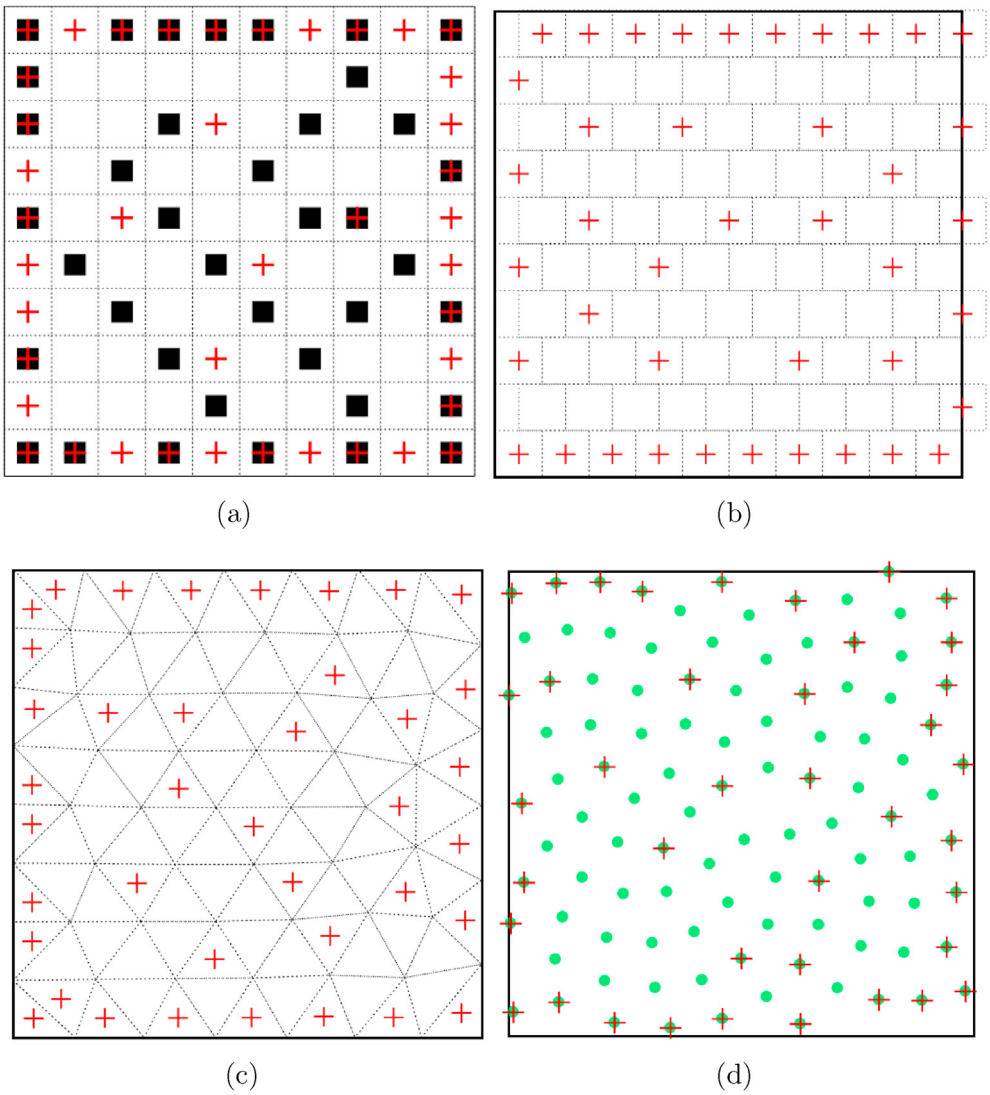

Fig. 6. Optimal layouts obtained from different potential turbine positions for (a) aligned mesh, (b) staggered mesh, (c) unstructured mesh and (d) sunflower mesh, respectively for case I. Filled squares: Grady et al. [7]; Red crosses: present results; Green dots: potential positions for the sunflower mesh approach. (For interpretation of the references to colour in this figure legend, the reader is referred to the Web version of this article.)

Table 2
Characteristics of the optimal layouts obtained from different configurations of potential turbine positions for case II.

	Aligned [7]	Aligned	Staggered	Unstructured	Sunflower
Obj (1/kW, $\times$ 10^{-3})	1.5666	1.5093	1.5147	1.5273	1.5155
P_{total} (kW)	17220	18596	18529	17627	18519
η (%)	85.17	87.49	87.18	87.19	87.13
N	39	41	41	39	41

affect the power production of wind farms as examined in Table 3. On the other hand, turbine-added turbulence in turbine wake also affects the fatigue loads on downwind turbines. The downwind turbines shown in Fig. 8 (a) and (b) may suffer a significant increase on fatigue loads on blades and the tower. The downwind turbines shown in Fig. 8 (c) and (d), on the other hand, may suffer partial loads on blades. Such fatigue loads are affected by both wake shear-layer induced turbulence and turbulence due to wake meandering, which cannot be accurately modeled using analytical models yet, and should be considered in further development of the proposed approach.

4. Conclusions and future work

Optimal turbine layout design is critical for the performance of wind farms. In this work, a physics-informed approach is proposed based on the classic work by Mosetti et al. [5] and Grady et al. [7] for the optimization of wind farm layouts, which employs the genetic algorithm for optimization and Jensen wake model with quadratic superposition for the effects of turbine wakes on wind farm performance. In the proposed approach, the physical understanding, that a staggered arrangement can produce more power than an aligned arrangement, is introduced to the design of potential

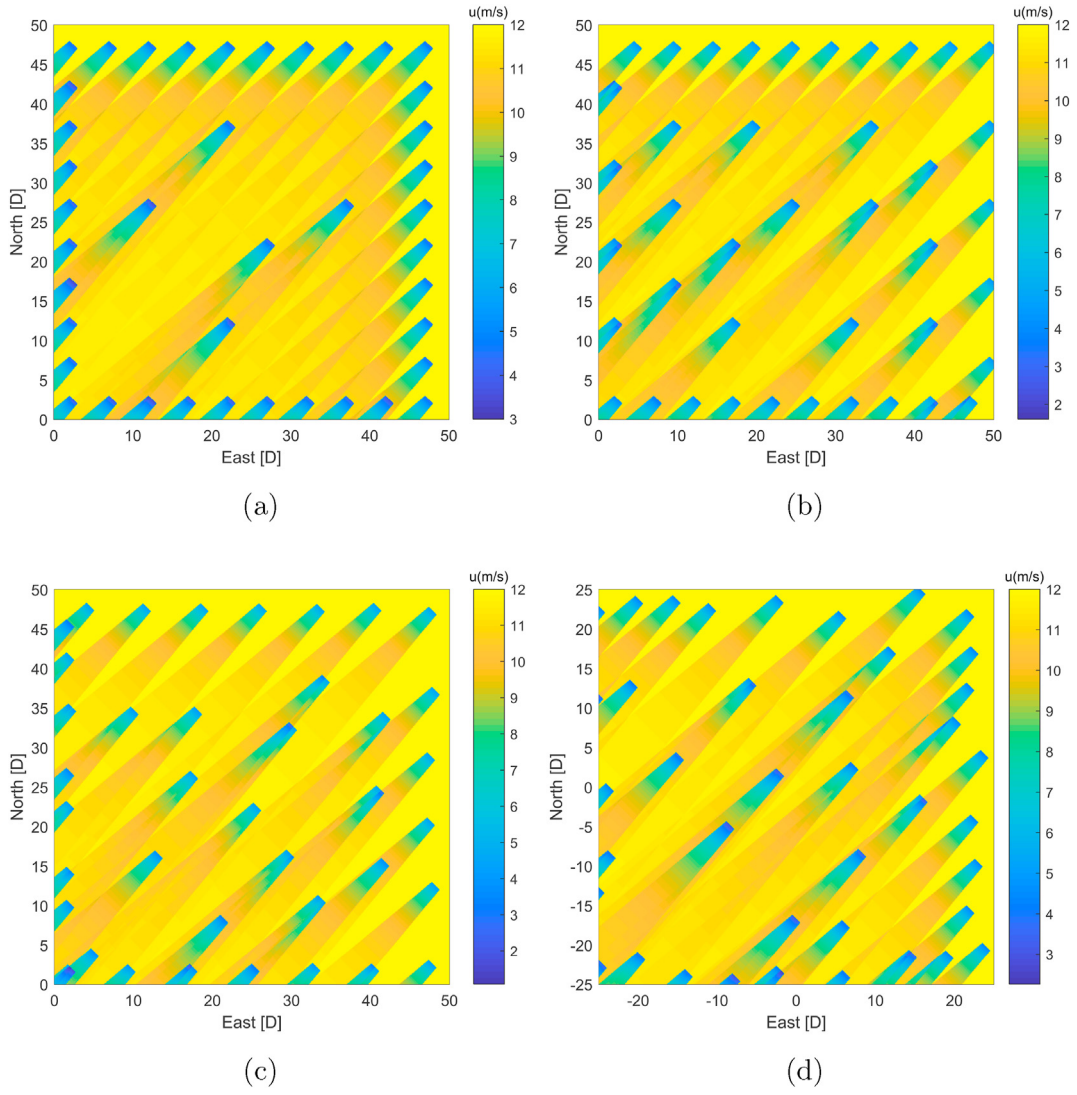

Fig. 7. Contours of downwind velocity for (a) optimal layout from the aligned mesh, (b) optimal layout from the staggered mesh, (c) optimal layout from the unstructured mesh, and (d) optimal layout from the sunflower mesh, respectively for case II. For the plotted wind field, the wind blows from the north-east direction.

Table 3
Performance of the optimal layouts obtained from case I under off-design conditions, in which the wind blows from the east direction perpendicular with the wind direction in case I.

	Aligned	Staggered	Unstructured	Sunflower
Obj (1/kW, $\times$ 10^{-3})	3.1500	2.9403	1.8315	1.7452
P_{total} (kW)	7012	9350	14699	16417
η (%)	45.09	45.09	72.71	75.40

turbine positions. This idea is tested through three different meshes, i.e. the staggered mesh, the unstructured mesh and the sunflower mesh and applied them to two cases for case I, uniform wind blowing from one direction, and case II, uniform wind evenly blowing from different directions. For case I, the performance of the optimal layouts from the staggered mesh and the sunflower mesh is higher than that of the other two layouts. For case II, the performance of the four different optimal layouts is similar with each other. The performance of the optimal layouts obtained in case I was also tested for off-design conditions. The off-design performance of the layouts obtained from the unstructured mesh and the sunflower mesh is observed better than the other two layouts. Based on the results from the two cases, the sunflower mesh for generating potential turbine locations is recommended for real-life scenarios.

The proposed approach needs to be further developed to include other crucial aspects and design variables in order to solve realistic WFLO problems. This work employs a very simple cost model and only maximizes the power production of the wind farm. Multiple criteria need to be considered [51] in the future work, such as noise [52,53], cost of the infrastructure [54] and operation & maintenance cost [55]. Additionally, for offshore wind farms, the approach needs to consider the cost related with foundation [56], which is affected by scour at seabed around the foundation and determines the region where wind turbine can be installed. For the design of potential turbine positions, only ideal wind conditions (i.e. unidirectional wind and uniform distribution of wind direction) are tested for different meshes. How to design the optimal potential turbine positions for different wind roses needs further investigation. Furthermore, only wind farms of square shape is considered in

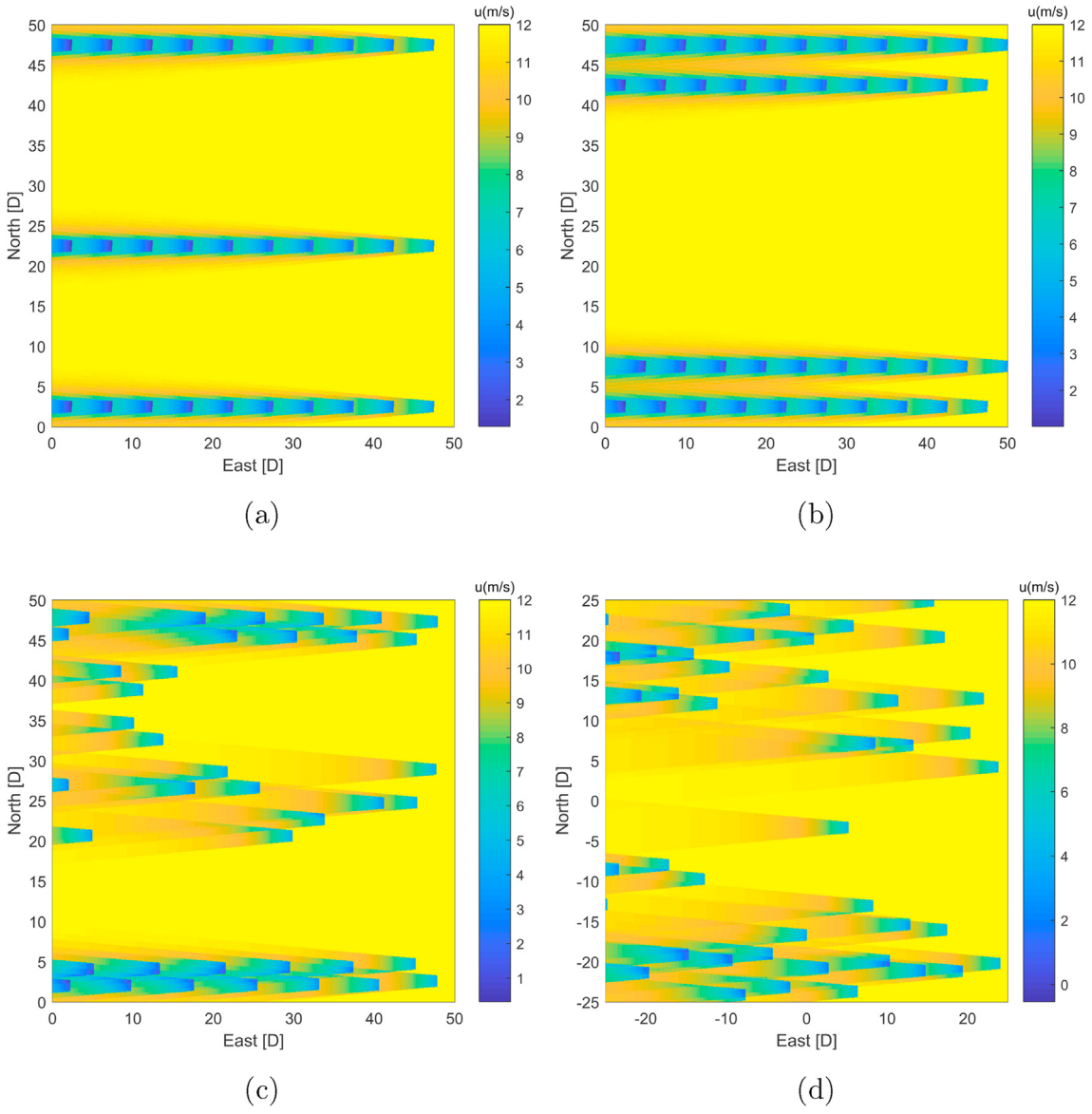

Fig. 8. Off-design test on the optimal layouts from case I. Contours of downwind velocity for (a) optimal layout from the aligned mesh, (b) optimal layout from the staggered mesh, (c) optimal layout from the unstructured mesh, and (d) optimal layout from the sunflower mesh. In this off-design test for the optimal layouts from case I, the wind blows from east.

this work. Work needs to be done for wind farms of irregular shapes and with restrictions [57]. Besides potential turbine positions, the shape of the wind farm can also be optimized by taking into account the characteristics of wind resources before the optimization of turbine positions [58]. In terms of applications, only horizontal axis wind turbines are considered in this work. The proposed methodology in principle can be extended to other energy harvesting technologies, such as the vertical axial wind turbine [59,60], hydrokinetic turbines [61,62] and wave energy collectors [63].

CRediT authorship contribution statement

Chutian Wu: Methodology, Software, Investigation, Validation, Visualization, Writing - original draft. **Xiaolei Yang:** Conceptualization, Methodology, Investigation, Project administration, Supervision, Resources, Writing - review & editing. **Yaxin Zhu:** Resources, Writing - review & editing.

Declaration of competing interest

The authors declare that they have no known competing financial interests or personal relationships that could have appeared to influence the work reported in this paper.

Acknowledgement

This work is partially supported by NSFC Basic Science Center Program for “Multiscale Problems in Nonlinear Mechanics” (NO. 11988102).

Appendix A. Effects of mesh refinement on optimal layouts

In this appendix, the optimization performance on finer meshes is examined for both case I and case II for the four different meshes. In the cases presented in section 3, there are approximately 100 potential turbine positions. In the cases tested in this appendix, approximately 400 potential turbine positions are employed for the four meshes, with other setups the same as those for case I and case II, respectively.

The optimal layouts obtained from refined meshes are shown in Figures A.9 and A.10 for case I and case II, respectively. For case I with unidirectional wind direction, it is observed that all turbines are placed at the inlet and the outlet of the domain for all four meshes. For the staggered mesh and sunflower mesh, it is observed that more turbines are placed near the inlet. With the refinement of the mesh, the performance is improved with increased number of wind turbines for the four different meshes as shown in Table A.4. Because of the smaller spacing between adjacent turbines in the transverse direction, it can be expected that the performance of the turbine layout will be significantly reduced when wind blows in the transverse direction. For case II with uniformly distributed wind directions, the performance is slightly improved as shown in Table A.5, which is not as significant as that for case I. The distribution of the optimal turbine positions is also changed with relatively less turbines placed in the central area of the domain. It is noticed that the optimal layouts from the staggered mesh are not the same as those from the refined aligned mesh for both case I and case II.

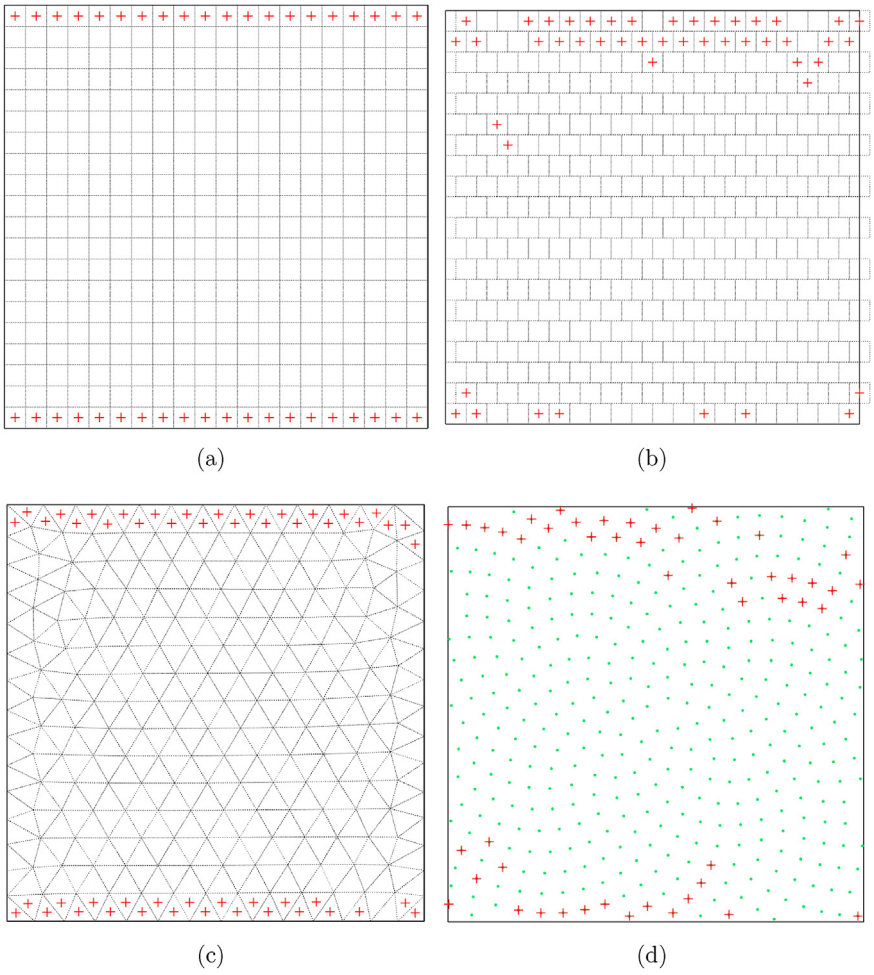

Fig. A.9Grid refinement study for case I: optimal layouts obtained from (a) aligned mesh, (b) staggered mesh, (c) unstructured mesh and (d) sunflower mesh with approximately 4 times potential turbine positions more than those in section 3.1.

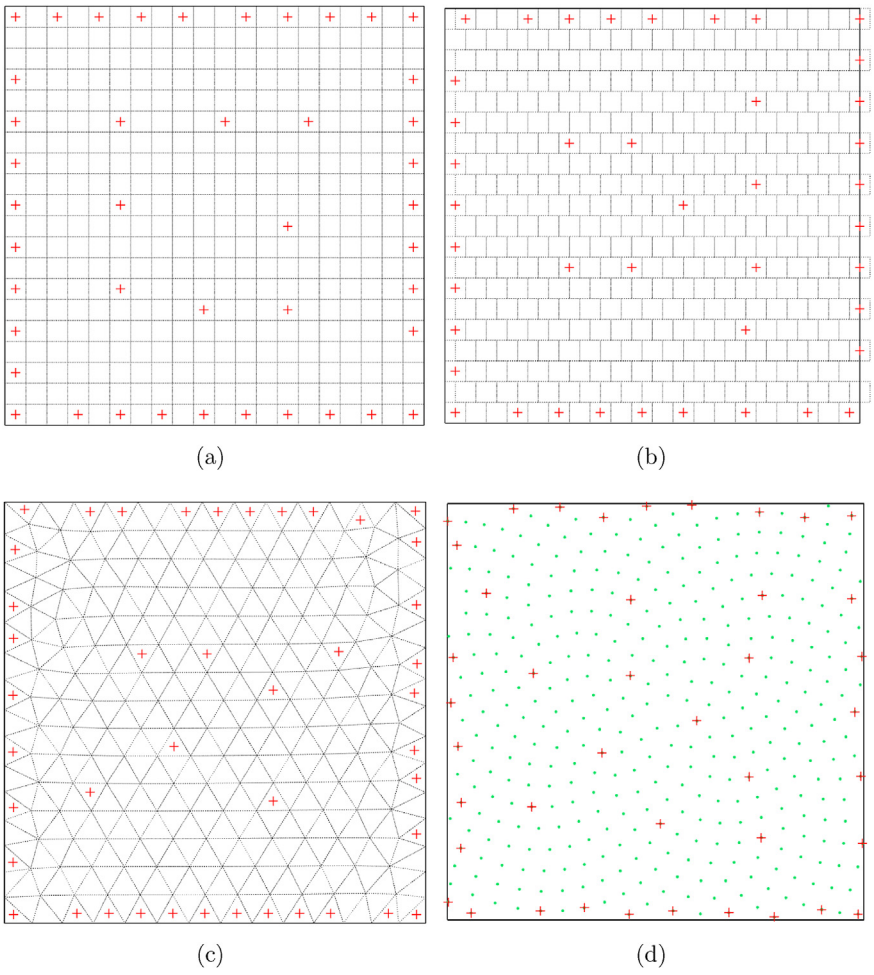

Fig. A.10Optimal layouts obtained from different refined potential turbines for (a) aligned mesh, (b) staggered mesh, (c) unstructured mesh and (d) sunflower mesh, respectively for case II. Potential positions are four times more than those in section 3.2.

Table A.4Grid refinement study for case I: characteristics of the optimal layouts obtained from meshes with approximately 4 times potential turbine positions.

	Aligned	Staggered	Unstructured	Sunflower
Obj (1/kW, $\times$ 10^{-3})	1.3688	1.3210	1.3424	1.3420
P_{total} (kW)	20083	23973	25464	24527
η (%)	96.85	98.39	96.32	96.56
N	40	47	51	49

Table A.5Grid refinement study for case II: characteristics of the optimal layouts obtained from meshes with approximately 4 times potential turbine positions.

	Aligned	Staggered	Unstructured	Sunflower
Obj (1/kW, $\times$ 10^{-3})	1.4877	1.4861	1.4912	1.4961
P_{total} (kW)	19654	19278	19608	19150
η (%)	88.17	88.54	87.96	87.95
N	43	42	43	42

References

[1] P. Veers, K. Dykes, E. Lantz, S. Barth, C.L. Bottasso, O. Carlson, A. Clifton, J. Green, P. Green, H. Holttinen, D. Laird, V. Lehtomäki, J.K. Lundquist, J. Manwell, M. Marquis, C. Meneveau, P. Moriarty, X. Munduate, M. Muskulus, J. Naughton, L. Pao, J. Paquette, J. Peinke, A. Robertson, J.S. Rodrigo, A.M. Sempreviva, J.C. Smith, A. Tuohy, R. Wiser, Grand challenges in the science of wind energy, Science 366 (6464) (2019).
[2] S. Rajper, I.J. Amin, Optimization of wind turbine micrositing: a comparative study, Renew. Sustain. Energy Rev. 16 (8) (2012) 5485–5492.
[3] Y. Ma, H. Yang, X. Zhou, J. Li, H. Wen, The dynamic modeling of wind farms considering wake effects and its optimal distribution, in: 2009 World Non-grid-connected Wind Power and Energy Conference, 2009, pp. 1–4.
[4] R. Shakoor, M.Y. Hassan, A. Raheem, N. Rasheed, M.N.M. Nasir, Wind farm layout optimization by using definite point selection and genetic algorithm, in: 2014 IEEE International Conference on Power and Energy, PECon, 2014, pp. 191–195.
[5] G. Mosetti, C. Poloni, B. Diviacco, Optimization of wind turbine positioning in large windfarms by means of a genetic algorithm, J. Wind Eng. Ind. Aerod. 51 (1) (1994) 105–116.
[6] Y. Eroğlu, S.U. Seçkiner, Design of wind farm layout using ant colony algorithm, Renew. Energy 44 (2012) 53–62.
[7] S. Grady, M. Hussaini, M. Abdullah, Placement of wind turbines using genetic algorithms, Renew. Energy 30 (2) (2005) 259–270.
[8] A. Emami, P. Noghreh, New approach on optimization in placement of wind turbines within wind farm by genetic algorithms, Renew. Energy 35 (7) (2010) 1559–1564, special Section: IST National Conference 2009.
[9] S. Pookpunt, W. Ongsakul, Optimal placement of wind turbines within wind farm using binary particle swarm optimization with time-varying acceleration coefficients, Renew. Energy 55 (2013) 266–276.
[10] S. Turner, D. Romero, P. Zhang, C. Amon, T. Chan, A new mathematical programming approach to optimize wind farm layouts, Renew. Energy 63 (2014) 674–680.
[11] J.M.C.N. Elkinton, J.F. Manwell, Optimization algorithms for offshore wind farm micrositing, in: Proceedings of the WINDPOWER 2007 Conference and Exhibition, 2007, pp. 3–6. Los Angeles, CA, USA.
[12] N. Jensen, A Note on Wind Generator Interaction, Risø National Laboratory,

1983. Risø–M–2411.
[13] M. Bastankhah, F. Porté-Agel, A new analytical model for wind-turbine wakes, Renew. Energy 70 (2014) 116–123.
[14] R.J.A.M. Stevens, D.F. Gayme, C. Meneveau, Coupled wake boundary layer model of wind-farms, J. Renew. Sustain. Energy 7 (2) (2015), 023115.
[15] X. Yang, F. Sotiropoulos, Analytical model for predicting the performance of arbitrary size and layout wind farms, Wind Energy 19 (7) (2016) 1239–1248.
[16] M. Ge, Y. Wu, Y. Liu, Q. Li, A two-dimensional model based on the expansion of physical wake boundary for wind-turbine wakes, Appl. Energy (2019) 975–984.
[17] X. Gao, H. Yang, L. Lu, Optimization of wind turbine layout position in a wind farm using a newly-developed two-dimensional wake model, Appl. Energy 174 (2016) 192–200.
[18] G.C. Larsen, H.A. Madsen, F. Bingöl, J. Mann, S. Ott, J.N. Sørensen, V. Okulov, N. Troldborg, M. Nielsen, K. Thomsen, et al., Dynamic Wake Meandering Modeling, Risø National Laboratory, 2007. Risø–R–1607.
[19] J. Ainslie, Development of an eddy viscosity model for wind turbine wakes, in: Proceedings of 7th BWEA Wind Energy Conference, 1985. Oxford.
[20] A. Crespo, F. Manuel, D. Moreno, E. Fraga, J. Hernandez, Numerical analysis of wind turbine wakes, in: Workshop on Wind Energy Applications, Delphi, Greece, 1985, pp. 15–25.
[21] D. Astolfi, F. Castellani, L. Terzi, A study of wind turbine wakes in complex terrain through rans simulation and scada data, Journal of Solar Energy Engineering-transactions of The ASME 140 (3) (2018) 31001.
[22] L.L. Tian, W.J. Zhu, W.Z. Shen, J.N. Sørensen, N. Zhao, Investigation of modified AD/RANS models for wind turbine wake predictions in large wind farm, in: 5th International Conference on the Science of Making Torque from Wind, vol. 524, 2014, p. 12151 (1) (2014).
[23] G.V. Iungo, F. Viola, U. Ciri, M.A. Rotea, S. Leonardi, Data-driven rans for simulations of large wind farms, J. Phys. Conf. 625 (1) (2015) 12025.
[24] J. Sumner, G. Espana, C. Masson, S. Aubrun, Evaluation of rans/actuator disk modelling of wind turbine wake flow using wind tunnel measurements, Int. J. Eng. Syst. Model Simulat. 5 (2013) 147.
[25] M. Calaf, C. Meneveau, J. Meyers, Large eddy simulation study of fully developed wind-turbine array boundary layers, Phys. Fluids 22 (1) (2010) 15110.
[26] Y.T. Wu, F. Porté-Agel, Large-eddy simulation of wind-turbine wakes: evaluation of turbine parametrisations, Boundary-Layer Meteorol. 138 (3) (2011) 345–366.
[27] D. Yang, C. Meneveau, L. Shen, Large-eddy simulation of offshore wind farm, Phys. Fluids 26 (2) (2014) 25101.
[28] X. Yang, F. Sotiropoulos, A new class of actuator surface models for wind turbines, Wind Energy 21 (5) (2018) 285–302.
[29] D. Foti, X. Yang, F. Campagnolo, D. Maniaci, F. Sotiropoulos, Wake meandering of a model wind turbine operating in two different regimes, Physical Review Fluids 3 (5) (2018) 54607.
[30] S. Frandsen, On the wind speed reduction in the center of large clusters of wind turbines, J. Wind Eng. Ind. Aerod. 39 (1–3) (1992) 251–265.
[31] X. Yang, F. Sotiropoulos, A review on the meandering of wind turbine wakes, Energies 12 (24) (2019).
[32] J. Meyers, C. Meneveau, Large eddy simulations of large wind-turbine arrays in the atmospheric boundary layer, in: 48th AIAA Aerospace Sciences Meeting Including the New Horizons Forum and Aerospace Exposition, 2010.
[33] X. Yang, F. Sotiropoulos, Les investigation of infinite staggered wind-turbine arrays, 4th Scientific Conference on the Science of Making Torque from Wind 555 (1) (2014) 12109.
[34] L.P. Chamorro, R.E. Arndt, F. Sotiropoulos, Turbulent flow properties around a staggered wind farm, Boundary-Layer Meteorol. 141 (3) (2011) 349–367.
[35] N. Hamilton, M. Melius, R.B. Cal, Wind turbine boundary layer arrays for cartesian and staggered configurations-part i, flow field and power measurements, Wind Energy 18 (2) (2015) 277–295.
[36] J. Koh, E. Ng, Downwind offshore wind turbines: opportunities, trends and technical challenges, Renew. Sustain. Energy Rev. 54 (2016) 797–808.
[37] H. Vogel, A better way to construct the sunflower head, Math. Biosci. 44 (3) (1979) 179–189.
[38] T. Göçmen, P. van der Laan, P.-E. Réthoré, A.P. Diaz, G.C. Larsen, S. Ott, Wind turbine wake models developed at the technical university of Denmark: a review, Renew. Sustain. Energy Rev. 60 (2016) 752–769.
[39] A. Crespo, J. Hernandez, S. Frandsen, Survey of modelling methods for wind turbine wakes and wind farms, Wind Energy: An International Journal for Progress and Applications in Wind Power Conversion Technology 2 (1) (1999) 1–24.
[40] R.J. Stevens, C. Meneveau, Flow structure and turbulence in wind farms, Annu. Rev. Fluid Mech. 49 (2017).
[41] X. Yang, F. Sotiropoulos, A review on the meandering of wind turbine wakes, Energies 12 (24) (2019) 4725.
[42] F. Porté-Agel, M. Bastankhah, S. Shamsoddin, Wind-turbine and wind-farm flows: a review, Boundary-Layer Meteorol. 174 (1) (2020) 1–59.
[43] P. Mittal, K. Kulkarni, K. Mitra, A novel hybrid optimization methodology to optimize the total number and placement of wind turbines, Renew. Energy 86 (2016) 133–147.
[44] L.Y. Pao, K.E. Johnson, A tutorial on the dynamics and control of wind turbines and wind farms, in: 2009 American Control Conference, IEEE, 2009, pp. 2076–2089.
[45] G. Marmidis, S. Lazarou, E. Pyrgioti, Optimal placement of wind turbines in a wind park using Monte Carlo simulation, Renew. Energy 33 (7) (2008) 1455–1460.
[46] M. Beşkirli, İ. Koç, H. Haklı, H. Kodaz, A new optimization algorithm for solving wind turbine placement problem: binary artificial algae algorithm, Renew. Energy 121 (2018) 301–308.
[47] J.S. González, A.G.G. Rodriguez, J.C. Mora, J.R. Santos, M.B. Payan, Optimization of wind farm turbines layout using an evolutive algorithm, Renew. Energy 35 (8) (2010) 1671–1681.
[48] S. Pookpunt, W. Ongsakul, Optimal placement of wind turbines within wind farm using binary particle swarm optimization with time-varying acceleration coefficients, Renew. Energy 55 (2013) 266–276.
[49] J. Feng, W.Z. Shen, Solving the wind farm layout optimization problem using random search algorithm, Renew. Energy 78 (2015) 182–192.
[50] A.M. Abdelsalam, M. El-Shorbagy, Optimization of wind turbines siting in a wind farm using genetic algorithm based local search, Renew. Energy 123 (2018) 748–755.
[51] D. Guirguis, D.A. Romero, C.H. Amon, Gradient-based multidisciplinary design of wind farms with continuous-variable formulations, Appl. Energy 197 (2017) 279–291.
[52] W. Yin Kwong, P. Yun Zhang, D. Romero, J. Moran, M. Morgenroth, C. Amon, Multi-objective wind farm layout optimization considering energy generation and noise propagation with nsga-ii, J. Mech. Des. 136 (9) (2014).
[53] J. Cao, W. Zhu, W. Shen, Z. Sun, Wind farm layout optimization with special attention on noise radiation, in: Journal of Physics: Conference Series, vol. 1618, IOP Publishing, 2020, 042022.
[54] C. Elkinton, J. Manwell, J. McGowan, Offshore wind farm layout optimization (owflo) project: preliminary results, in: 44th AIAA Aerospace Sciences Meeting and Exhibit, 2006, p. 998.
[55] M.A. Lackner, C.N. Elkinton, An analytical framework for offshore wind farm layout optimization, Wind Eng. 31 (1) (2007) 17–31.
[56] A.G. Gonzalez-Rodriguez, Review of offshore wind farm cost components, Energy for Sustainable Development 37 (2017) 10–19.
[57] H. Sun, H. Yang, X. Gao, Investigation into spacing restriction and layout optimization of wind farm with multiple types of wind turbines, Energy 168 (2019) 637–650.
[58] J. Feng, W.Z. Shen, Co-optimization of the shape, orientation and layout of offshore wind farms, in: Journal of Physics: Conference Series, vol. 1618, IOP Publishing, 2020, 042023.
[59] T.D. Ashwill, Measured Data for the Sandia 34-meter Vertical axis Wind Turbine, Sandia National Laboratories, Albuquerque, NM 87185, 1992.
[60] M. Borg, A. Shires, M. Collu, Offshore floating vertical axis wind turbines, dynamics modelling state of the art. part i: Aerodynamics, Renew. Sustain. Energy Rev. 39 (2014) 1214–1225.
[61] X. Yang, A. Khosronejad, F. Sotiropoulos, Large-eddy simulation of a hydrokinetic turbine mounted on an erodible bed, Renew. Energy 113 (2017) 1419–1433.
[62] M. Musa, C. Hill, F. Sotiropoulos, M. Guala, Performance and resilience of hydrokinetic turbine arrays under large migrating fluvial bedforms, Nature Energy 3 (10) (2018) 839–846.
[63] F. Taveira-Pinto, P. Rosa-Santos, T. Fazeres-Ferradosa, Marine renewable energy, Renew. Energy 150 (2020) 1160–1164.